AGU ADVANCING EARTH AND SPACE SCIENCES

Earth's Future

RESEARCH ARTICLE
10.1029/2024EF004549

National-Scale Flood Hazard Data Unfit for Urban Risk Management

Jochen E. Schubert[1], **Katharine J. Mach**[2,3], **and Brett F. Sanders**[1,4]

[1]Department of Civil and Environmental Engineering, University of California, Irvine, Irvine, CA, USA, [2]Department of Environmental Science and Policy, Rosenstiel School of Marine, Atmospheric, and Earth Science, University of Miami, Miami, FL, USA, [3]Leonard and Jayne Abess Center for Ecosystem Science and Policy, University of Miami, Coral Gables, FL, USA, [4]Department of Urban Planning and Public Policy, University of California, Irvine, Irvine, CA, USA

Abstract Extreme flooding events are becoming more frequent and costly, and impacts have been concentrated in cities where exposure and vulnerability are both heightened. To manage risks, governments, the private sector, and households now rely on flood hazard data from national-scale models that lack accuracy in urban areas due to unresolved drainage processes and infrastructure. Here we assess the uncertainties of First Street Foundation (FSF) flood hazard data, available across the U.S., using a new model (PRIMo-Drain) that resolves drainage infrastructure and fine resolution drainage dynamics. Using the case of Los Angeles, California, we find that FSF and PRIMo-Drain estimates of population and property value exposed to 1%- and 5%-annual-chance hazards diverge at finer scales of governance, for example, by 4- to 18-fold at the municipal scale. FSF and PRIMo-Drain data often predict opposite patterns of exposure inequality across social groups (e.g., Black, White, Disadvantaged). Further, at the county scale, we compute a Model Agreement Index of only 24%—a ∼1 in 4 chance of models agreeing upon which properties are at risk. Collectively, these differences point to limited capacity of FSF data to confidently assess which municipalities, social groups, and individual properties are at risk of flooding within urban areas. These results caution that national-scale model data at present may misinform urban flood risk strategies and lead to maladaptation, underscoring the importance of refined and validated urban models.

Plain Language Summary Flooding presents a significant risk to human activities and development, and its impacts have been rapidly increasing over recent decades. However, government flood mapping in the U. S. has not kept pace with adaptation needs, and communities have now turned to other sources of information to inform planning and design decisions. This study examines the uncertainties of flood hazard data available from the First Street Foundation across Los Angeles, California, the second largest city in the U.S. With a comparison to two different models that more fully capture processes known to affect urban flooding, we show concerning levels of uncertainty in the First Street Foundation data at scales of municipalities and properties. These results highlight the need for more robust validation of urban flood hazard models, and caution against overreliance of First Street Foundation data for urban flood management.

Key Points:

- Flood risks are concentrated in urban areas, where national-scale hazard models are less accurate
- Flood exposure estimates become increasingly uncertain at finer scales and may misrepresent the social distribution of risk
- Refined and validated urban flood models are needed to effectively and equitably manage increasingly severe flood risks

Supporting Information:

Supporting Information may be found in the online version of this article.

Correspondence to:

B. F. Sanders,
bsanders@uci.edu

Citation:

Schubert, J. E., Mach, K. J., & Sanders, B. F. (2024). National-scale flood hazard data unfit for urban risk management. *Earth's Future*, *12*, e2024EF004549. https://doi.org/10.1029/2024EF004549

Received 22 FEB 2024
Accepted 17 JUN 2024
Corrected 5 AUG 2024

This article was corrected on 5 AUG 2024. See the end of the full text for details.

Author Contributions:

Conceptualization: Jochen E. Schubert, Katharine J. Mach, Brett F. Sanders
Formal analysis: Jochen E. Schubert, Brett F. Sanders
Funding acquisition: Jochen E. Schubert, Katharine J. Mach, Brett F. Sanders
Investigation: Jochen E. Schubert, Brett F. Sanders
Methodology: Jochen E. Schubert, Brett F. Sanders
Writing – original draft: Jochen E. Schubert, Katharine J. Mach, Brett F. Sanders

1. Introduction

Federal efforts to map flood hazards in the U.S. have been inadequate for meeting the full needs for risk management including risk awareness, preparedness, risk transfer, and incorporation of future changes in hazards related to climate change (National Research Council, 2009). Flood hazard maps communicate information about the severity of flooding that is possible with extreme (i.e., rare) events, and are instruments for public safety, insurance pricing, asset management, land use regulation and many other applications (Serra-Llobet et al., 2022). In particular, Federal Emergency Management Agency (FEMA) Flood Insurance Rate Maps (FIRMs) developed for regulatory and insurance purposes in the U.S. do not capture all hazard drivers, have been updated too infrequently to keep pace with changes in land use and climate, and do not capture future changes in flood hazards (Bates et al., 2021). The private sector has stepped in to fill this void, developing models and data products that aim to more completely, accurately, and nimbly estimate present and future flood risks (Bates et al., 2021; Harris, 2023), which are rapidly changing (O'Donnell & Thorne, 2020). The urgent need for this information is clear: financial-services industries and federal insurance programs have rapidly adopted these data products, yet with seemingly little concern about potential inadequacies (Harris, 2023).

Writing – review & editing: Jochen E. Schubert, Katharine J. Mach, Brett F. Sanders

Most saliently, the First Street Foundation (FSF) has developed a national-scale flood hazard data set for the U.S. that has been used for risk communication to the public, insurance pricing, and scientific research about flood risks and inequities (First Street Foundation, 2020; Tate et al., 2021; Wobus et al., 2021) and the effect of flood risk on population growth (Shu et al., 2023). FSF data are now featured in many tools and programs for flood risk management and environmental justice (Harris, 2023) including the Environmental Justice Screening and Mapping Tool (EJScreen) developed by the U.S. Environmental Protection Agency (EPA, 2023), and the White House Climate and Environmental Justice Screening Tool (Council on Environmental Quality, n.d.). States have adopted FSF data for statewide resilience and risk reduction planning and have taken advantage of the property-specific aspects of FSF data to implement resilience measures such as buyouts (Duncan et al., 2023). Moreover, FEMA has relied on flood hazard data from many sources, including large-scale flood risk models used in the insurance industry, to implement Risk Rating 2.0—a program to align insurance rates with actuarial risks on a property-by-property basis—within the National Flood Insurance Program (FEMA, 2022). Within the real-estate industry, FSF data are increasingly relied upon for property-level risk assessment by buyers, realtors, and lenders (Realtors Property Resource, n.d.; Redfin, 2024). However, researchers have cautioned against over-reliance on large-scale hazard model data for flood management decision-making needs, particularly at increasingly fine spatial scales (Bates, 2023a), because of uncertainties stemming from the inadequate representation of topographic features, flood infrastructure, and other features known to affect patterns of flooding (Jonkman, 2013; Trigg et al., 2016; Ward et al., 2015).

How uncertain are these national-scale flood hazard data now being extensively deployed within the public and private sectors? A widely used metric of flood hazard data uncertainty is the Model Agreement Index (MAI), which quantifies the fraction of agreement between hazard models in areas at risk of flooding; MAI = 100% would indicate perfect agreement (Trigg et al., 2016). Wing et al. (2017) compared flood extent estimated by the U.S.-wide flood hazard model adopted by FSF to FEMA flood hazard maps and reported an MAI of 55% for the nation as a whole, but also a trend of decreasing accuracy with increasing levels of urbanization. Wing et al. (2017) reported MAI values of 33%, 24%, and 23% within areas classified by the National Land Cover Database as "Developed: low intensity," "Developed: medium intensity," and "Developed: high intensity," respectively. Lindersson et al. (2021) examined global-scale differences between flood maps developed by the European Commission's Joint Research Center (Dottori et al., 2016) and by the Global Assessment Report on Disaster Risk Reduction (Rudari et al., 2015), and reported a global MAI of only 30%. Uncertainties in large scale hazard models are particularly high in cities given the complexity of interacting factors that affect flooding, including topography, urban drainage infrastructure, and flood defenses such as levees and flood walls (Bates, 2023a). Moreover, data describing these features are not widely available to support more accurate modeling (Bates, 2023a; Trigg et al., 2016; Ward et al., 2015), and data availability at global scales present an even greater challenge.

From a flood management perspective, these trends in model accuracy present a serious concern: large-scale hazard model uncertainty is greatest precisely where population density is greatest. The implications for understanding flood risks, pricing properties, shaping policy, and prioritizing flood adaptation measures may be profound, with implications for environmental justice. Uncertainties in flood hazard data propagate through estimates of flood exposure, damages, and social inequalities used in flood adaptation decision-making processes, as flood hazard data are intersected with spatially explicit social data including the locations of housing, population densities, racial and ethnic population fractions, and indicators of socioeconomics, social vulnerability, and neighborhood disadvantage.

Here we use two models that benefit from more detailed local data and a more complete accounting of processes known to affect flooding to measure the degree of flood risk uncertainty in FSF data at the scale of properties, municipalities, and the county of Los Angeles, California. The second largest city in the U.S., Los Angeles has experienced numerous flooding disasters during its development over the past two centuries and faces significant flood risk linked to atmospheric rivers and undersized main-stem flood channels (Figure 1a) (Huang & Swain, 2022; Sanders et al., 2023). A Parallel Raster Inundation Model (PRIMo) is configured to more fully capture features known to affect flooding, compared to FSF data—including urban topography, urban drainage infrastructure, flood walls, and levees—based on access to high quality local infrastructure and topographic data (Bates, 2023b; Kahl et al., 2022; Sanders et al., 2023; Sanders & Schubert, 2019). A second model, PRIMo-Drain, is configured to also account for the effect of local street drains on pluvial flooding (see Methods). With three separate flood hazard data sources representative of 1%- and 5%-annual-chance scenarios, we compare metrics

10.1029/2024EF004549

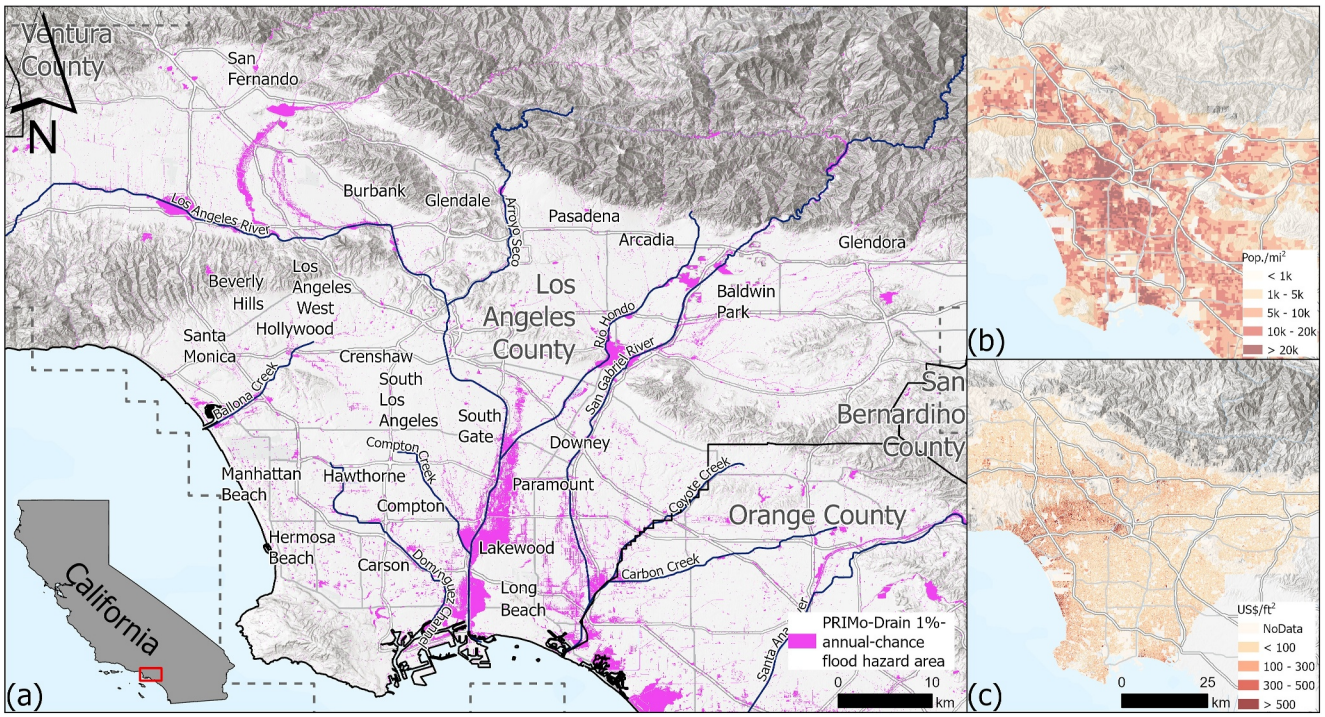

Figure 1. Los Angeles study area including: (a) Topographic relief (shading), major road network (light gray lines), main-stem flood channels (dark blue), county boundaries (dashed gray lines), and municipal boundaries (heavy gray lines) with 1%-annual-chance flood hazard area (pink), (b) population density, and (c) property value. Flood extent based on PRIMo-Drain model using a 30 cm depth threshold.

that bear on flood management and environmental justice including exposed populations and property values at county and municipal scales; inequalities in exposure at the county scale by race, ethnicity and disadvantage; and flood extent, which provides a measure of risk uncertainty at the property scale.

2. Materials and Methods

2.1. Site Description and Parcel Data

Los Angeles (LA) County, California is home to a population of 9.8 million people (U.S. Census Bureau) and a gross domestic product of 712 billion USD (U.S Bureau of Economic Analysis), making it larger than 40 U.S. states by population and 43 by economic output. Positioned on a coastal plain below the San Gabriel Mountains, the region is exposed to fluvial flood risks from mountain runoff, pluvial flooding from intense rainfall and coastal flooding hazards (Jones, 2018; Sanders & Grant, 2020). Data on flood hazards, land use, lot area, property value, population, income, race, ethnicity, disadvantage, and vulnerability were characterized across 1,767,588 land parcels to enable regional and municipal scale exposure analysis. Land parcels represent the smallest unit of land for the purpose of ownership. Flood hazard, land use, lot area, and property values were resolved for each parcel, and all other variables were downscaled from 2020 U.S. Census data at the block group and/or census tract scale. Tracts generally have population sizes of 1,200–8,000, and block groups are divisions of census tracts that generally contain 600–3,000 people (U. S. Census Bureau, 2022).

Parcel shapefiles with lot area, land use, and Assessor's value were accessed from the Los Angeles County Open Data Portal (Los Angeles County, n.d.). Population was estimated dasymetrically by apportioning the block group population from the 2020 Census across residential parcels in proportion to lot area (Tate et al., 2021), and zero population was ascribed to commercial or other parcel types. Each residential parcel was also assigned a Black, Hispanic, and White population fraction corresponding to the block group fraction computed from Census data (Figure 2). We note that U.S. Census data include separate questions related to race (e.g., Black, Asian, Native American) and ethnicity (Hispanic), and these data are used directly such that there is overlap between race and ethnicity in the evaluation of exposure and inequalities. The study area population is 9,105,286 which by ethnicity is 48.2% Hispanic and by race is 49% White, 22.0% other, 14.2% Asian, 8.6% Black, 4.4% Two or More Races,

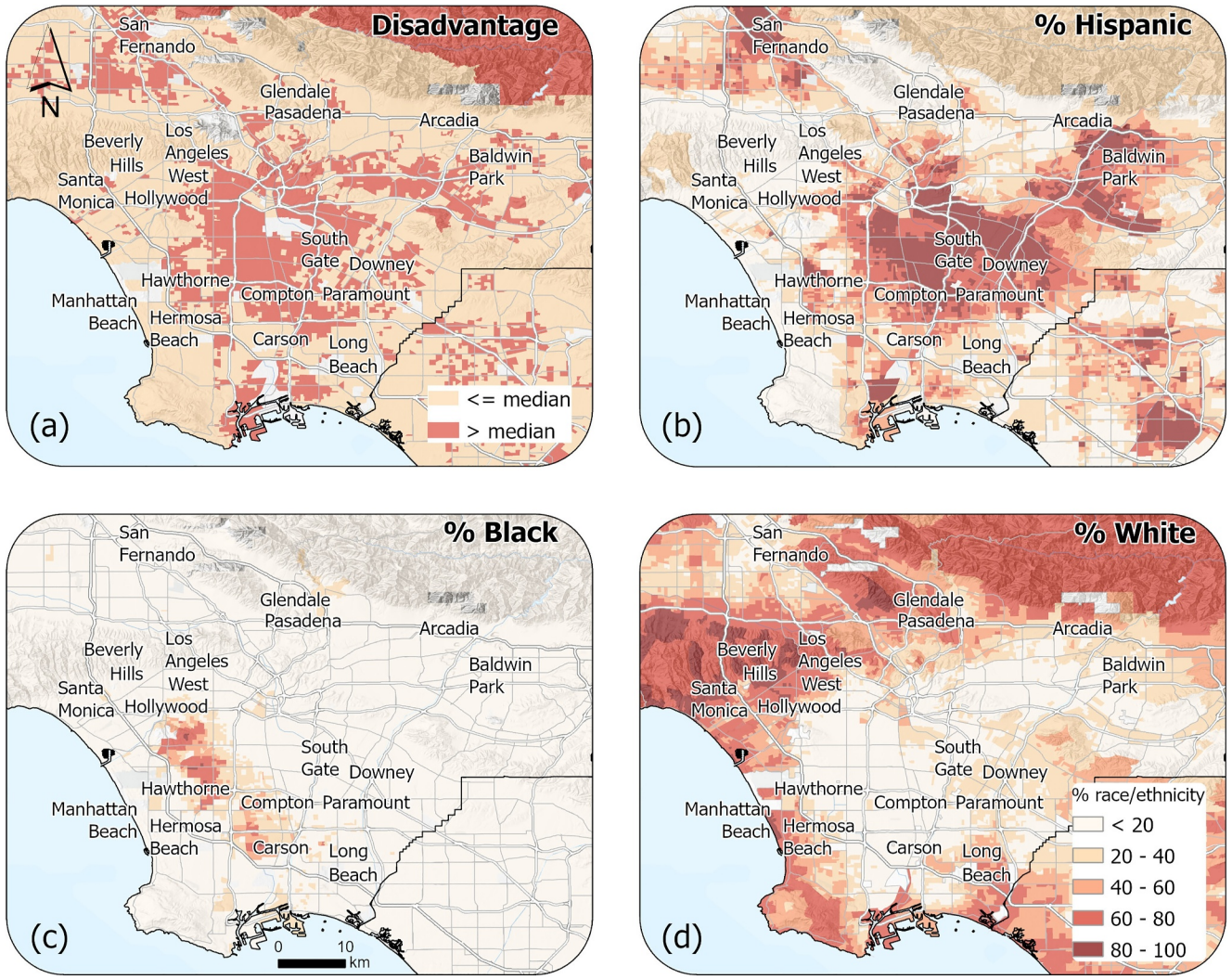

Figure 2. Spatial distribution of social groups across Los Angeles County. (a) Disadvantaged populations as estimated by the Neighborhood Disadvantage Index (NDI > median), (b) Hispanic population fraction, (c) Black population fraction (by race alone), and (d) White population fraction (by race alone). All population fractions reference the same color scale. Population fractions based on U.S. Census data, and NDI developed from U.S. Census and American Community Survey (ACS).

0.7% Native American, and 0.3% Hawaii and other Pacific Islander. Each residential parcel was also assigned a Neighborhood Disadvantage Index (NDI), which is a block group scale measure of socioeconomic disadvantage that varies from zero to one and was developed from literature on neighborhood disadvantage, urban and concentrated poverty, neighborhood effects, and residential segregation (Sanders et al., 2023). The 5th, 50th, and 95th percentile value of NDI for Los Angeles County is 0.35, 0.47 and 0.59, respectively (Sanders et al., 2023). Analysis of exposure and inequalities focuses on four social groups: White (by race), Black (by race), Hispanic, and Disadvantaged defined by NDI greater than the county median. Distributions of these social groups are shown in Figure 2. Exposure of Asian populations was also examined and did not reveal strong inequalities; Asian groups were therefore not a focus of detailed analysis.

2.2. FSF Flood Hazard Data

We accessed 5%- and 1%-annual-chance FSF flood depth data available in a 3 m resolution georeferenced raster format. FSF flood depth data are produced using the LISFLOOD-FP model for pluvial and fluvial flood risk and the GeoCLAW model for coastal flood risk (First Street Foundation, 2020). LISFLOOD-FP solves the local-inertia-only formulation of the 2D shallow water equations (Bates et al., 2010; Sampson et al., 2013) and

switches to different governing equations in areas where the assumptions of the local-inertial-only formulation are violated, such as on steep slopes where a slope-dependent variable-velocity rainfall routing scheme is applied (First Street Foundation, 2020; Sampson et al., 2013). Infiltration of rainfall runoff across pervious surfaces is modeled using a modified Hortonian infiltration equation, applied in conjunction with the Harmonized World Soil Database (HWSD) of the Food and Agriculture Organization of the United Nations (FAO) (First Street Foundation, 2020). The LISFLOOD-FP simulations are executed on a 30 m national elevation data (NED) digital elevation model (DEM), which was hydroconditioned using hydrologic drainage information from the NHDPlus and MERIT data sets to synthetically correct the slopes of major river channels (First Street Foundation, 2020). For channels with widths at or less than the DEM resolution, a one-dimensional (1D) subgrid method is applied to create a flow routing pathway (Neal et al., 2012). Engineered structures, such as dams and levees as is the case across Los Angeles, are incorporated in different ways in the modeling strategy. Levees, which typically are narrower than the DEM resolution, are incorporated in the model using a framework of channel conveyance increase based on estimates of local defense standards (Sampson et al., 2015). In the case of dams, if LISFLOOD-FP predicts flooding within a dam's service area for a scenario that has an annual-chance greater than the safety standard of the dam, then that flooding is removed from the LISFLOOD-FP outputs as a post-processing step. Dam service areas are obtained from each dam's Emergency Action Plan. FSF derives other flood protection measures such as culverts, elevated roads, and stormwater systems/pipes from FEMA Flood Insurance Study (FIS) reports (First Street Foundation, 2020). We note that across the Los Angeles metropolitan region, FIS reports are primarily available along watercourses and coastal regions, but very few are available across the urban core. Wing et al. (2017) report that for the U.S. national LISFLOOD-FP model, urban drainage is accounted for by assuming a design standard depending on the degree of urbanization, based on luminosity data (Elvidge et al., 2007), and the duration and intensity of the event. However, available documentation does not describe the regional data sources used for each region of the U.S.

Precipitation forcing data for the FSF flood hazard data considered here are provided by NOAA's Atlas 14 Intensity-Duration-Frequency (IDF) (Perica et al., 2014) relationships for the 24 hr rainfall duration at various return periods. While FSF has recently moved toward a new set of precipitation intensity data reflective of the most recently climatic conditions (Kim et al., 2023), the data considered here are based on NOAA Atlas 14 forcing. Fluvial floods hazards are forced in the LISFLOOD-FP model at a set of inflow boundary conditions derived using the regionalized flood frequency analysis (RFFA) methodology outlined by Smith et al. (2015) and updated for the U.S. as described in the FSF Technical manual (First Street Foundation, 2020). A two step-approach is used to create hydrographs for extreme flow events: first an index flood is estimated, and second the index flood is scaled using growth curves that describe the relationship between index flood and extreme flow. To create the index flood, gauges were partitioned by river or hydrological zone and their discharge record is used to calculate the mean annual flood for each zone. To calculate the growth curves, gauging stations are subdivided into the five categories of the Koppen-Geiger climate classification and pooled together based on catchment homogeneity. For each pooled group of gages, extreme value distributions are fitted to the gaged streamflow data, providing relationships between the index flood and extreme flows for any recurrence interval. The methodology was developed for global flood hazard modeling and in particular to bridge streamflow gaps in data scarce regions. Smith et al. (2015) report that large errors in extreme flow estimation can occur in data scarce regions, greater than 300% in some cases (global mean error of approx. 80%), although across the denser streamflow gaging network of the Los Angeles metropolitan region errors are likely smaller. To counteract the potentially large errors in extreme flow estimates using the RFFA methodology, FSF uses a framework of channel conveyance scaling, whereby estimated bankfull discharge or local degree of protection (e.g., levees) is utilized to calibrate the estimated extreme flow (First Street Foundation, 2020).

GeoCLAW predicts storm surge and tidal flood hazard using the 2D shallow water equations with the addition of source terms for wind friction, non-constant surface pressure and Coriolis (Mandli & Dawson, 2014). GeoCLAW uses adaptive mesh refinement with overlapping rectangular grids to allow greater detail along the coast while maintaining computational efficiency and stability. Ocean bathymetry and coastal topography in the model are parameterized using the global SRTM15+v2 DEM with linear spatial resolution of 500 m, although finer resolution lidar DEMS from NOAA and USGS are integrated into the model where available along coastlines. Storm surge in GeoCLAW is determined by a specification of the storm's wind field through time, and energy from the wind field is transferred to the water through drag. Tides are predicted using each NOAA tide gage station's harmonic constituents (First Street Foundation, 2020). While GeoCLAW doesn't model wave run-up, the outputs

of the model are post-processed using a statistical model that was established by comparing USGS observations of flood height to GeoCLAW model outputs.

Flood depths are downscaled from LISFLOOD-FP and GeoCLAW to a finer resolution through a two-step process. First, water surface elevation is resampled at a fine resolution, and second, flood depth is estimated by subtracting topographic height from surface water elevation (First Street Foundation, 2020).

2.3. PRIMo Flood Hazard Modeling

The Parallel Raster Inundation Model (PRIMo) solves the full 2D shallow-water equations using a dual-grid finite volume scheme that combines a fine-resolution grid of topography for spatial accuracy with a coarse-resolution grid for efficient time integration (Kahl et al., 2022; Sanders & Schubert, 2019). The PRIMo model for Los Angeles previously reported by Sanders et al. (2023) is adopted here as a baseline model for flood hazard assessment. The baseline model has a 3 m resolution fine-grid (DEM) to resolve topography and updates the solution in time on a 30 m grid. The DEM was constructed mainly from two sources, 1/9th arc second (3 m) USGS National Elevation Data set (NED) DEM (primarily from 2016 lidar data (OCM Partners, 2022)) for elevations above 10 m and a 1 m resolution USGS topobathymetric DEM for elevations less than 10 m NAVD 88 including coastal bathymetry. The DEM was hydroconditioned to account for culverts, subsurface storm drains, dams and levees (Sanders et al., 2023). To model flow resistance, a 3 m resolution raster grid model of the Manning coefficient was developed based on land use data available from OpenStreetMap and tabulated values of the Manning parameter for each land use category (Sanders et al., 2023). No infiltration was assumed in PRIMo simulations because urban areas in the study area are marked by a high level of imperviousness, and because extreme flooding events are typically associated with persistent rainfall that saturates the ground surface prior to episodes of extreme rainfall lasting hours (Sanders & Grant, 2020). With hydro-conditioning of the DEM, the baseline PRIMo model is configured to account for Level 1 drainage infrastructure which corresponds to regional flood control dams and the main-stem flood channels with levees, as well as Level 2 drainage infrastructure which corresponds to secondary flood conveyance structures including channels and underground culverts.

A second model, PRIMo-Drain, is introduced here to account for Level 3 drainage infrastructure in the assessment of pluvial flood hazards, in addition to Level 1 and 2 infrastructure. Level 3 infrastructure corresponds to local street drains and small conveyance pipes that transfer drainage into Level 2 drainage infrastructure. Data describing the location of street drain inlets were obtained from the County of Los Angeles (Los Angeles County Public Works, n.d.), and each drain was configured as a curb inlet with a length of 2 m and a height of 0.2 m (Gallegos et al., 2009). Across the study area, a total of 153,280 curb drain inlets were included in the model. Inlet flow rates, Q_{drain}, were modeled with a mix of weir and orifice equations (Leandro et al., 2009), an approach that was successfully used in past-studies of flood inundation in Los Angeles County (Gallegos et al., 2009; Sanders & Schubert, 2019). Specifically, flow is based either on a weir-type equation or an orifice-type equation depending on the local flood depths, d, and curb height, H_{curb}, as follows,

$$Q_{\text{drain}} = \begin{cases} c_D L d\sqrt{gd} & d < H_{\text{curb}} \\ c_D L H_{\text{curb}}\sqrt{2gd} & d \geq H_{\text{curb}} \end{cases}$$

where L represents the horizontal length of the curb drain inlet and c_D represents a dimensionless discharge coefficient expected in the range of 0.1–0.5 (Gallegos et al., 2009). A calibration process was used to estimate c_D: a single, spatially-uniform value was identified such that flood inundation predicted for the 5% annual chance event is largely (at least 90%) contained within street curbs, a criterion that approximates the design specifications for urban drainage infrastructure described in the Los Angeles County Hydrology Manual (Conkle et al., 2006). To measure whether simulations achieve the design criteria, we computed the fraction of the flooded area with a depth greater than 0.3 m, the approximate height of street curbs, within a calibration subdomain of the entire study area (Figure S1 in Supporting Information S1). A depth criterion was used because PRIMo pluvial flood simulations result in relatively deep flooding within the street network and relatively shallow flooding outside the street network, and it is straightforward to quantify flood depths. The goal to "largely" (>90%) contain deep flooding (>0.3 m) was achieved by reducing the deep-flooding fraction to 10%. Calibration resulted in $c_D = 0.14$, which achieved a deep-flood fraction of 9.5%. By comparison, PRIMo predicts a deep-flood fraction of 27.7% for

the 5% annual chance event. The calibration was tested within two validation subdomains where the flood fraction was found to be 9.8% and 13.1%. Text S1 in Supporting Information S1 provides a more detailed description of the calibration and validation process, Figure S1 in Supporting Information S1 shows the flooding distribution with the calibration and validation sub-domains using PRIMo and PRIMo-Drain, and Table S1 in Supporting Information S1 summarizes all statistics on the fraction of flooded area with depths greater than 0.3 m. The existing drainage infrastructure data from the County of Los Angeles (Los Angeles County Public Works, n.d.) do not allow for matching inlets with their corresponding outlets, so inlet flows are not routed into the mainstem flood channels for consideration as a possible fluvial hazard. Importantly, fluvial flood hazard scenarios along mainstem flood channels are configured using extremes in streamflow rates estimated from gage records, as described next, so routed drainage flows are unnecessary.

PRIMo and PRIMo-Drain were applied to simulate the 5%- and 1%-annual-chance flood hazard depths (at the 50th percentile) considering coastal, fluvial, and pluvial hazard drivers using the same methods reported by Sanders et al. (2023). Briefly, precipitation forcing is based on NOAA Atlas 14 data, fluvial forcing is based on frequency analysis of 51 different stream gages in the region, and coastal flooding is based on frequency analysis of annual maximum total water level measurements at the Los Angeles NOAA tide gage (9410660). Both the PRIMo and PRIMo-Drain models were configured to run using 756 tiles of raster grids of size 1,000 × 1,000, which corresponds to 756 million points.

2.4. Exposure and Inequality Analysis

Exposed populations and exposed property value are estimated by intersecting flood hazard distributions (Figure 1a) with population density (Figure 1b) and property value (Figure 1c) at the scale of land parcels, and by summing results at the scale of the county and municipalities. Flooded land parcels were defined by a depth threshold of 30 cm, a level that aligns with U.S. standards for flood hazard mapping (FEMA, 2018). Furthermore, exposed populations for each social group were estimated by summing the product of the parcel-level population and the corresponding ethnic/racial fractions in areas classified as flooded. For Disadvantaged exposure, the summation occurred across land parcels classified as flooded and Disadvantaged. Across the study area, there are 85 municipalities as defined by Los Angeles County Assessor tax codes (Figure 1a). Lorenz curves were developed at the County scale by sorting the parcel-level data set in accordance with a ethnic/racial fractions (or NDI for the Disadvantaged social group) and then building cumulative distribution functions (CDFs) for population (for the x-axis) and population-weighted flood hazard (for the y-axis) (Sanders et al., 2024). All CDFs were normalized by the maximum values so Lorenz curves scale from zero to unity on both axes. Furthermore, Gini coefficients are computed as indicators of inequality (Sanders et al., 2024).

Municipal scale flood severity is estimated by averaging the flood depth over land parcels with flood depth greater than 30 cm, and municipal scale Disadvantage is estimated by averaging the neighborhood disadvantage index (NDI) over land parcels with a flood depth greater than 30 cm.

Differences in exposure, E, between two models, A and B, across N municipalities are computed using the Geometric Mean Relative Error (GMRE), which is defined as follows,

$$\text{GRME}\,(A,B) = \exp\left(\frac{1}{N}\sum_{i=1}^{N}\log\left(\frac{(E_A)_i}{(E_B)_i}\right)\right)$$

Differences in flood extent predicted by two models, A and B, were estimating using MAI and Bias (Trigg et al., 2016),

$$\text{MAI}(A,B) = \frac{F_A \cap F_B}{F_A \cup F_B} \quad \text{Bias}(A,B) = \frac{F_A}{F_B}$$

where F_A and F_B represent the flood extent of models A and B, respectively, and flood extent was defined by 3 m resolution DEM cells with depth greater than 30 cm.

10.1029/2024EF004549

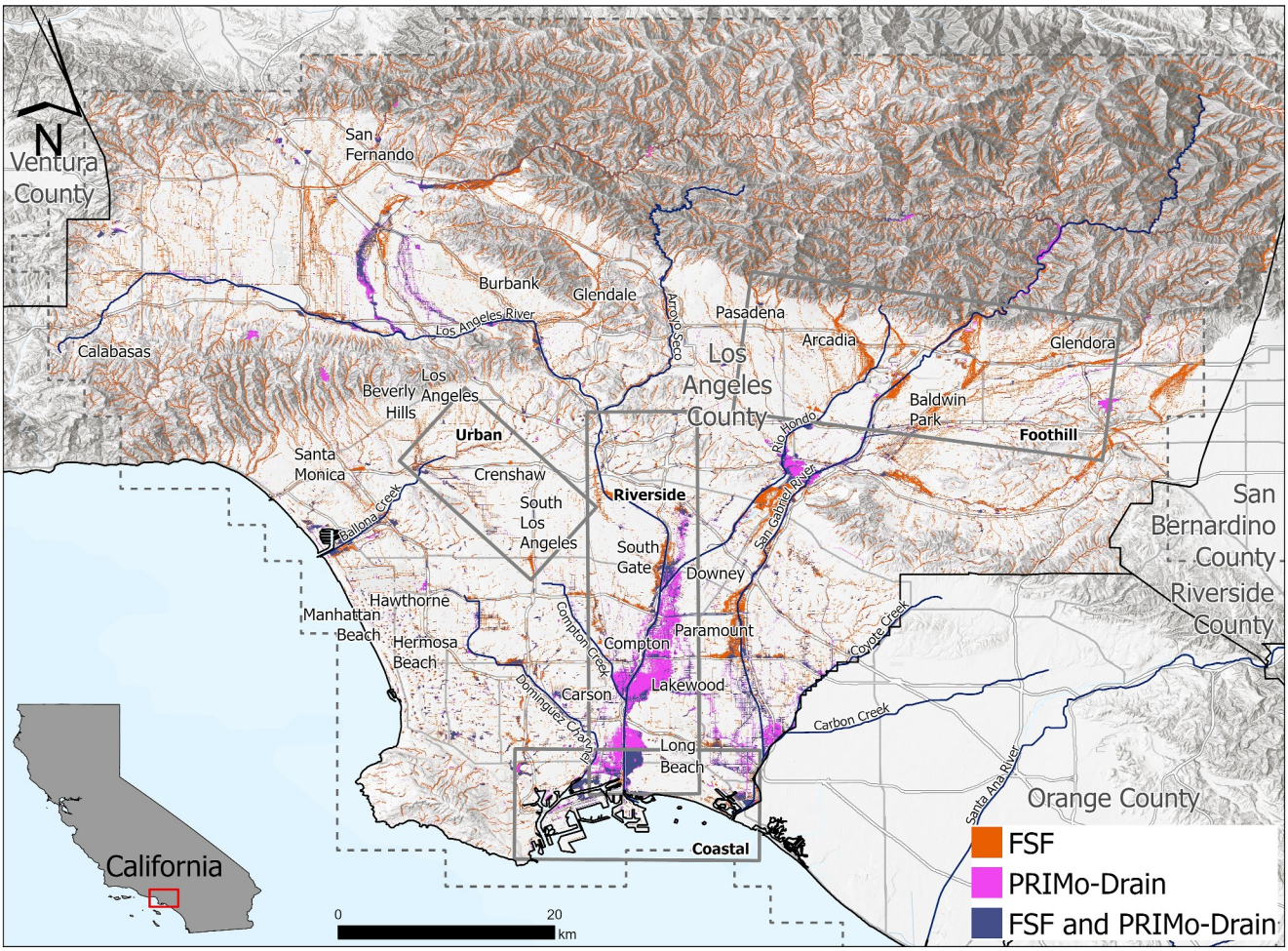

Figure 3. 1%-annual-chance flood extent estimated by FSF, PRIMo-Drain and both models using a 30 cm depth threshold. Model Agreement Index (MAI) = 20% at the county scale, with greater flood extent predicted by FSF in Foothill areas and greater flood extent predicted by PRIMo-Drain in the Riverside areas. Table 1 presents MAI and Bias tabulated for four geographical subdomains (Foothill, Urban, Riverside and Coastal) delineated by rectangles.

3. Results

3.1. Flood Extent MAI and Bias

Figure 3 shows the spatial distribution of the 1%-annual-chance flood extent predicted by the FSF data only, PRIMo-Drain data only, and both data sets, and Table 1 documents MAI and Bias between FSF, PRIMo and PRIMo-Drain at the county scale and within Foothill, Urban, Riverside, and Coastal subdomains for both the 1%- and 5%-annual-chance flood extent (Figure 3, gray rectangles). Focusing first on biases, results show that FSF data are biased toward greater flood extent in areas of greater topographic relief, as indicated by Bias = 1.91 and 2.57 between PRIMo and PRIMo-Drain, respectively, for the Foothill subdomain. Conversely, PRIMo and PRIMo-Drain are biased toward greater flood extent, relative to FSF data, along mainstem flood channels as indicated by Bias = 0.56 and 0.66, respectively, for the Riverside subdomain. With the 5%-annual-chance hazard, FSF data remain biased toward greater flood extent in areas of greater topographic relief (Table 1, Foothill subdomain), while PRIMo models remain biased toward greater flood extent along mainstem flood channels (Table 1, Riverside subdomain).

Secondly, PRIMo-Drain is biased toward less urban pluvial flooding under the 1%-annual-chance event compared to PRIMo and FSF data—a result of representing more than 100,000 storm drain inlets across Los Angeles County. Table 1 shows Bias = 3.15 for FSF flood extent compared to PRIMo-Drain flood extent in the Urban subdomain, while Bias = 1.03 when FSF flood extent is compared to PRIMo flood extent. Hence, FSF and

Table 1
Model Agreement Index (MAI) and Bias Comparing FSF Flood Extent to PRIMo and PRIMo-Drain Flood Extent for the 1% and 5% Annual-Chance Scenario

	1%-annual-chance				5%-annual-chance			
	FSF/PRIMo		FSF/PRIMo-drain		FSF/PRIMo		FSF/PRIMo-drain	
Spatial domain	MAI (%)	Bias	MAI (%)	Bias	MAI (%)	Bias	MAI (%)	Bias
Los Angeles County	24	1.91	20	2.57	16	1.55	16	1.90
Foothill	19	3.11	13	4.72	15	2.38	15	2.54
Urban	34	1.03	25	3.15	15	0.20	23	0.59
Riverside	34	0.56	32	0.66	15	0.22	18	0.33
Coastal	47	0.73	30	0.84	38	0.71	16	1.79

Note. Foothill, Urban, Riverside and Coastal geographies are shown in Figure 3.

PRIMo predict a similar amount of pluvial flooding. Conversely, under the 5%-annual-chance event, PRIMo-Drain predicts greater pluvial flooding than FSF data (Bias = 0.59 for Urban subdomain) and PRIMo also predicts much greater pluvial flooding than FSF data (Bias = 0.20 for Urban subdomain). The Hydrology Manual for Los Angeles County calls for urban drainage systems that are designed to contain flooding within street curbs from events with an annual frequency greater than 4% (Conkle et al., 2006), although that standard is not necessarily met across the entire region because responsibility for Level 3 infrastructure (curb inlets and small storm pipes) falls upon municipal governments and because some areas were developed before these standards were put into place. Nevertheless, large scale flood hazard models may assume that no flooding occurs with frequent events, while both PRIMo and PRIMo-Drain models route rainfall amounts to reveal a degree of flooding. As a consequence, urban pluvial flooding biases between PRIMo models and FSF data may reverse with changes in flood severity based on the representation of urban drainage.

MAI shown in Table 1 serves as a measure of flood extent accuracy at the property scale. For the 1%-annual-chance event, MAI is only 24% between FSF and PRIMo and 20% between FSF and PRIMo-Drain. An MAI value of 25% corresponds to a 1 in 4 chance that models agree on which properties are at risk in areas susceptible to flooding, which points to high model uncertainties relative to which properties are at risk. With the 5%-annual-chance event, MAI drops to 16% between FSF and PRIMo and between FSF and PRIMo-Drain. The MAI tends to be lowest in areas with more topographic relief (13%–19% across all models and scenarios in Foothill subdomain) and highest in coastal areas (16%–47% across all models and scenarios in Coastal subdomain). The MAI between FSF and PRIMo for the 1%-annual-chance event (24%) closely matches the value reported by Wing et al. (2017) for urban areas with high intensity development (MAI = 23%), and is slightly lower than global-scale differences in global flood hazard models (MAI = 30%) reported by Lindersson et al. (2021).

3.2. Exposed Population and Property at County and Municipal Scales

FSF and PRIMo estimates of population and property value exposed to 1%- and 5%-annual-chance hazards increasingly diverge at smaller scales relevant to governance. At the county scale overall, we find that population and property value estimated to be at risk of flooding by FSF and PRIMo models generally differ by 50% or less (Figures 4a and 4b), even though accuracy at property scale is low as shown by MAI values reported in Table 1. FSF and PRIMo hazard data point to 495 thousand and 425 thousand people, respectively, under a 1%-annual-chance hazard (Figure 4a), or a relative difference of 14%. Similarly, property value falling within the 1%-annual-chance flood zone is estimated to be 84.2 billion USD and 55.8 billion USD based on FSF and PRIMo data (Figure 4b), respectively, which represents a 34% difference. With the more frequent 5%-annual chance event, FSF and PRIMo data predict exposure of 120 thousand and 170 thousand people (Figure 4e), respectively—a 30% difference—and property value of 24.7 billion and 31.5 billion USD (Figure 4g), respectively—a 22% difference. With PRIMo updated to account for street drain inlets in the analysis of pluvial flooding (i.e., PRIMo-Drain), estimates of exposed populations and property values are reduced by 32% and 37%, respectively, under the 1%-annual-chance event (Figures 4a and 4b) and 47% and 40%, respectively, under the 5%-annual-chance event (Figures 4e–4g). Differences in county-scale exposure are generally similar or smaller than differences in

10.1029/2024EF004549

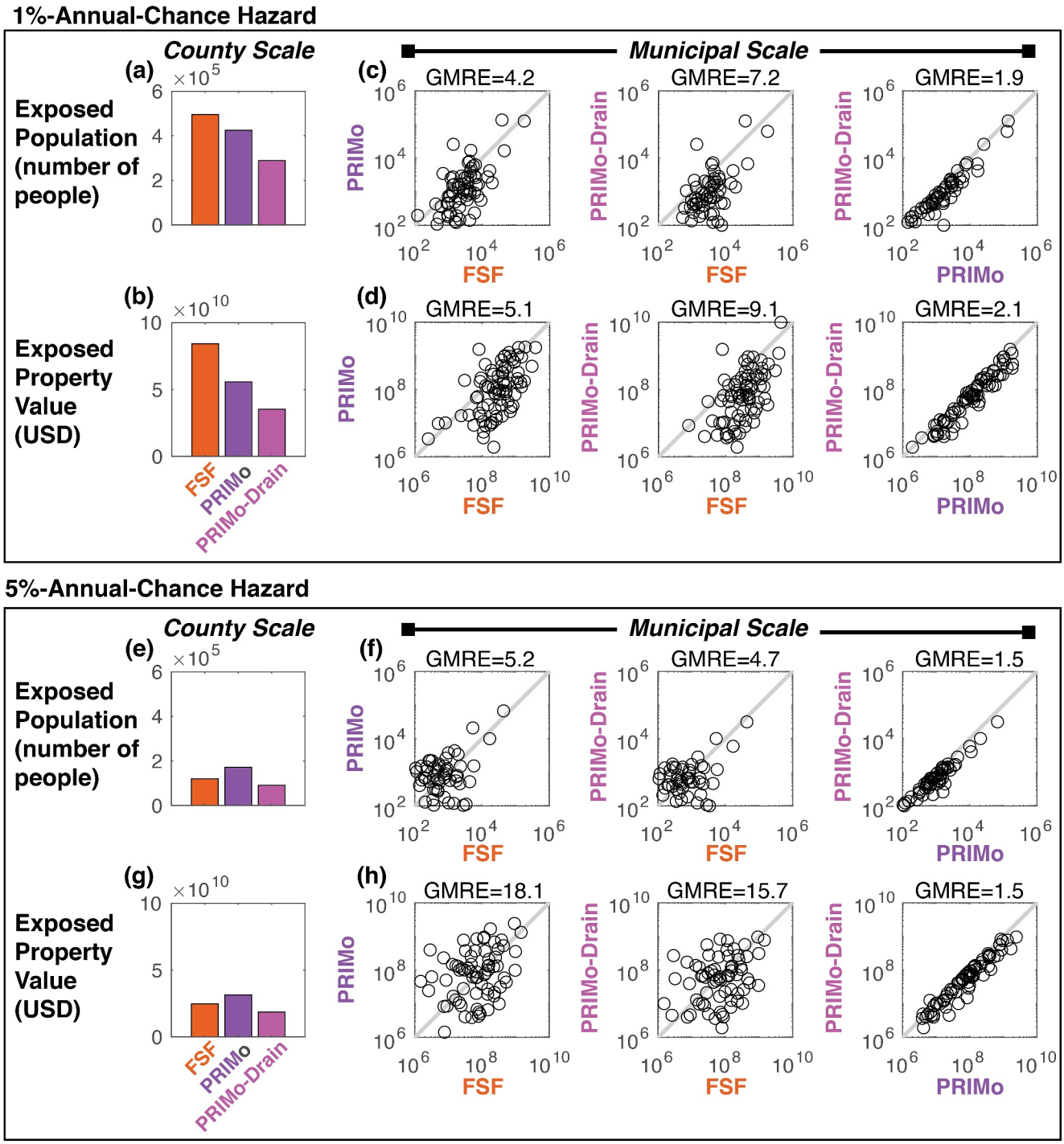

Figure 4. Estimates of flood exposure at county and municipal scales. 1%-annual-chance county-scale estimates of (a) exposed population and (b) exposed property value based on FSF, PRIMo, and PRIMo-Drain models. 1%-annual-chance municipal-scale estimates of (c) exposed people and (d) exposed property value based on FSF, PRIMo and PRIMo-Drain models. Panels (e–h) mirror (a–d), respectively, for the 5% annual-chance hazard. GMRE represents geometric mean relative error, a measure of relative difference. There are 85 municipalities (by tax code) in the study area.

exposure from uncertainty in the magnitude of the 1%-annual-chance flood peak, which suggest flood exposure range of −54% to +76% for the 5th and 95th percentile, respectively (Sanders et al., 2023).

Differences in exposure across hazard data sources are much higher at smaller municipal scales. We find four- and five-fold differences (Figures 4c and 4d) between FSF and PRIMo data based on Geometric Mean Relative Error

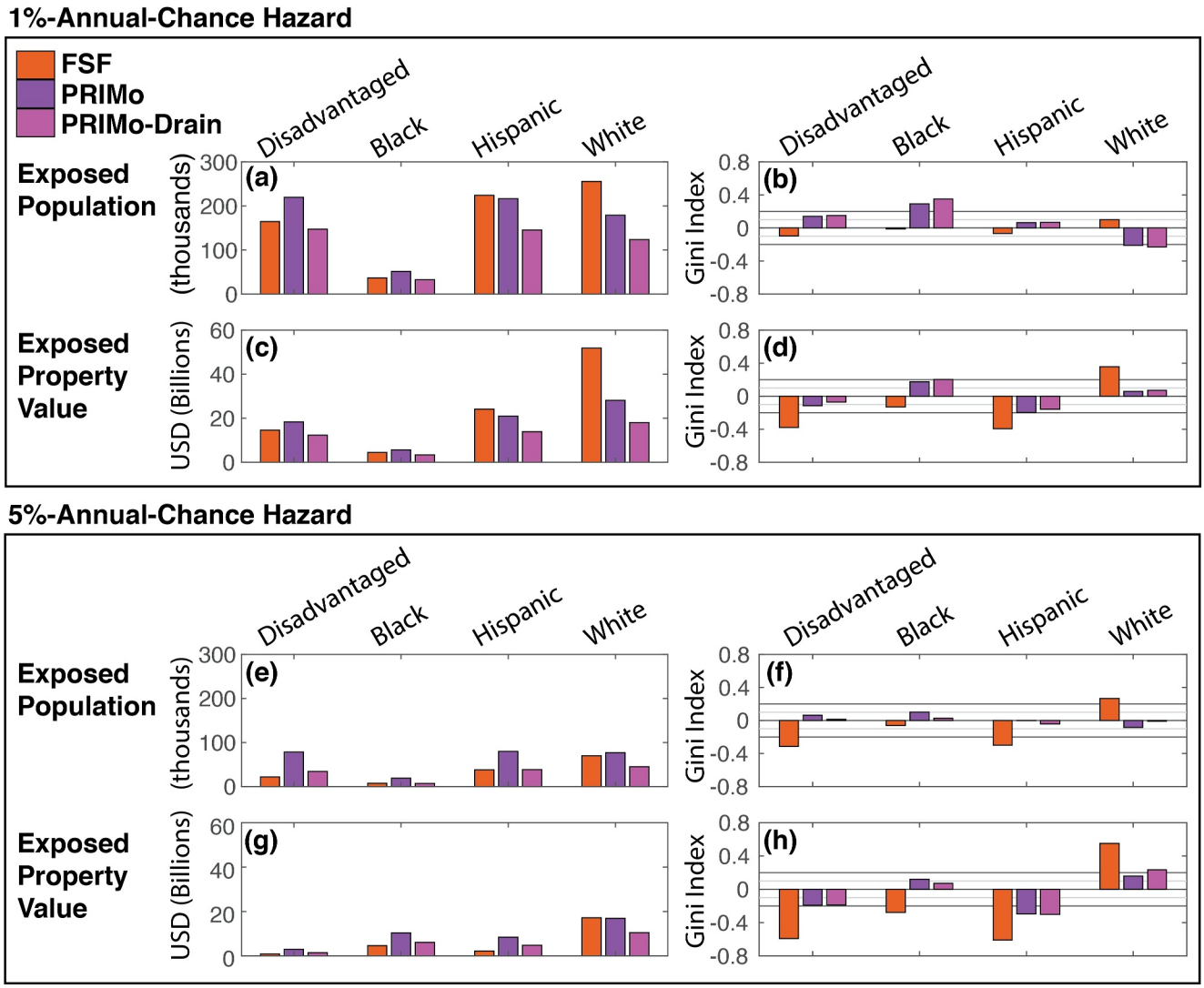

Figure 5. Estimates using FSF, PRIMo and PRIMo-Drain data of (a) exposed population by social groups, (b) Gini index of exposed populations by social groups, (c) exposed property value by social groups and (d) Gini index of exposed property value by social groups for the 1% annual-chance hazard. Panels (e–h) mirror (a–d), respectively, for the 5% annual-chance hazard. Gini index magnitude of 0.1 and 0.2 taken as threshold for weak and strong inequalities, respectively.

(GMRE). Differences between FSF and PRIMo-Drain data are even greater with GMRE = 7.2 (Figures 4c) and 9.1 (Figure 4d) for exposed population and property value, respectively. With the more frequent 5%-annual-chance hazard, municipal scale differences in exposed population are about five-fold (Figure 4f) between FSF and PRIMo (GMRE = 5.2) and also between FSF and PRIMo-Drain (GMRE = 4.7). Furthermore, differences in exposed property value are 18-fold (GMRE = 18.1) between FSF and PRIMo and 16-fold (GMRE = 15.7) between FSF and PRIMo-Drain. Differences between PRIMo and PRIMo-Drain are smaller, about two-fold or less, with GMRE = 1.9 (Figures 4c) and 2.1 (Figure 4d) under the 1%-annual-chance hazard for exposed population and property value, respectively, and GMRE = 1.5 for both exposed populations (GMRE = 1.5) and exposed property value at the 5%-annual-chance level.

3.3. Inequalities in Exposure by Social Groups

Differences in the spatial distribution of flood hazard data sets drive differences in estimates of exposure inequalities, with implications for environmental justice. We find that modest differences in number of people within each social group exposed to the 1%-annual-chance hazard point (Figure 5a) drive major differences in estimated inequalities (Figure 5b). Taking a Gini index magnitude of 0.1 and 0.2 as the threshold for "weak" and

"strong" inequalities, the PRIMo models point to strong inequality in exposure for Black populations, a strong level of underexposure for White populations, and a weak inequality for Disadvantaged populations. Conversely, the FSF data points to weak underexposure of Disadvantaged populations and weak inequality for White populations. Figure 5c shows the property value exposed by social groups across the hazard models, and notably the FSF data predict almost twice as much property value aligned with White populations compared to the PRIMo models. Indeed, the FSF data point to a strong inequality (Figure 5d) in property value exposure for White populations and strong underexposure of property value with Disadvantaged, Black, and Hispanic populations. We note here that residents are often not owners of property, and thus the exposure of property value and inequalities should be taken as indicators of community risk and not necessarily of resident risks. Both PRIMo models predict a weak level of underexposure for Hispanic populations, and the PRIMo model predicts a weak underexposure for Disadvantaged communities. Hence, there is agreement in the direction of the inequality between PRIMo and FSF for these social groups. However, for Black populations, the PRIMo models predict an inequality in the opposite direction compared to the FSF data. Note here that the formulation of the Lorenz curve for exposed population differs from the formulation for exposed property value, and this can lead to different patterns of inequalities across social groups (Sanders et al., 2024).

We also evaluated the exposed population (Figure 5e) and exposed property (Figure 5g) by social groups for the 5%-annual-chance hazards, and as before, inequalities predicted by the FSF data (Figures 5f and 5h) are substantially different from inequalities predicted by the PRIMo data. Indeed, the FSF data point to strong inequalities in exposure of people for White populations and strong underexposure for Disadvantaged and Hispanic populations, while the PRIMo models do not predict strong inequalities. Focusing on property value, FSF data point to very strong (Gini index magnitude greater than 0.5) inequalities for White populations, very strong underexposure for Disadvantaged and Hispanic populations, and strong underexposure for Black populations. The direction of the inequalities derived from the PRIMo data is aligned with those from the FSF data for Disadvantaged, Hispanic, and White populations, while the magnitudes are smaller with PRIMo data and the directions are opposite for Black populations.

4. Discussion

There are many sources of uncertainty in flood hazard models, and numerous researchers have emphasized that these uncertainties tend to amplify with increasing resolution (Alipour et al., 2022; Bates, 2023a; Dottori et al., 2013; Savage et al., 2016; Trigg et al., 2016). Our results show that exposed population and exposed property value estimated using three different flood hazard data sources for both 1%- and 5%-annual-chance scenarios differ overall by about a factor of two or less at the county scale, but that four- to seven-fold differences in exposed population and five- to 18-fold differences in exposed property value are predicted at municipal scales. Differences of this magnitude could radically reshape assessment of the geographic distribution of risk and priorities for flood projects and funding. Our results also show that inequalities in exposure estimated using different data sources result in nearly polar opposite assessments of whether a particular social group is disproportionately at risk or not, with implications for environmental justice. Finally, our results point to only 24% agreement in the spatial extent of the 1%-annual-chance flood zone, which suggests a 1 in 4 chance that individual properties at risk are confidently assessed as such and decisions related to specific properties could easily be misinformed.

Differences across data sources stem from a combination of different model structures and data sources. For example, PRIMo simulates fluvial flooding by routing the estimated flood peaks through channels with a fully two-dimensional solver and accounts for channel overtopping based on estimates of levee heights from lidar data and other sources. FSF models generally don't have access to local lidar data sets and other data to sharpen the representation of levees and instead make assumptions about channel capacity based on local flood defense standards (Sampson et al., 2015). Hence, FSF estimates of fluvial flooding may be strongly biased by uncertain estimates about flood defense standards (e.g., Smith et al., 2015). High bias in FSF data in the upper watershed (e.g., Foothill subdomain in Figure 3a), compared to PRIMo data, can be attributed to differences between models in the hydroconditioning of topographic data along streams (First Street Foundation, 2020) and routing of overland flow, including differences in topographic data (30 vs. 3 m DEM) and differences in the equations that are solved (see Methods). Similarly, low flood extent agreement (MAI $\sim$ 0.3) across the Urban subdomain geographies can be attributed to the effects of different DEMs and routing methodologies including the treatment of local drainage infrastructure. Whether similar, greater or lower levels of agreement between FSF and PRIMo

estimates of flood hazards would be measured across different regions and different geographies is difficult to say, but the aforementioned drivers of model differences offer some clues. For example, high levels of topographic relief and ground slopes appear to produce high bias, and high levels of dependence on assumed levels of protection from infrastructure do as well. Smaller differences between FSF and PRIMo predictions might then be expected in areas with less topographic relief and areas with lower levels of urbanization. Global comparisons of flood hazard models have pointed to areas of greater topographic relief and greater aridity—like Los Angeles—as geographies where model disagreement is particularly high (Lindersson et al., 2021).

It's likely that the PRIMo data are more accurate than the FSF data, but we can't say for sure. The PRIMo models follow methods known to improve the accuracy of urban flood inundation predictions including use of fine-resolution topographic data, information about levees and channel conditions, and information about storm water infrastructure such as culverts, subsurface pipes, and street drains (Bates, 2023b). The PRIMo model has also been qualitatively validated with comparisons to other local models (Sanders et al., 2023) and feedback from stakeholders (Ulibarri et al., 2023). Furthermore, PRIMo predictions align with past studies documenting the Black, Hispanic, and disadvantaged communities at risk along main-stem flood channels and in the lower watershed, especially (Orsi, 2004). Nevertheless, the degree of validation could be improved, and there remains an urgent need, as well as a challenge, to validate urban flood models nationwide and globally as others have suggested previously (Bates, 2012, 2023a; De Moel et al., 2015; Jonkman, 2013; Molinari et al., 2019; Trigg et al., 2016). The urgent need for urban flood validation data highlights the importance of emerging efforts to systematically monitor urban flooding at hyper-local scales (Gold et al., 2023; Son et al., 2023).

Opposite indications of exposure inequality across social groups, using FSF versus PRIMo hazard data, signal the need to carefully consider previous work documenting flood risk inequalities across the U.S. Previous work intersecting FSF data with social data has resulted in findings that hot spots of flood risk are located across rural areas of the Southeast (Tate et al., 2021), that poorer White populations are disproportionately at risk today (Wing et al., 2022), and that future flooding will disproportionately impact Black populations along the Gulf and Atlantic coasts (Wing et al., 2022). However, these assessments of present-day risk do not necessarily align well with the impacts of extreme flood events over recent decades, which have revealed major impacts to urban areas and disproportionate exposure and impacts for Black populations (Bullard & Wright, 2012; Chakraborty et al., 2019; Hornbeck & Naidu, 2014; Nguyen et al., 2023; Smiley, 2020). Across the U.S., historically underserved and socially vulnerable populations are concentrated within floodplains defended by levees (Vahedifard et al., 2023), and the actual levels of protection afforded by these levees may be different from the levels assumed to generate the FSF hazard data. Indeed, earlier work revealed that several main stem flood channels in Los Angeles are undersized to contain the 1%-annual-chance flood peak, yet this risk is not reflected in the FEMA flood maps for the region (Sanders et al., 2023).

The need for credible flood risk information is urgent. Effective flood risk management depends on robust, spatially explicit understanding of flood hazards, across the social scales of flood risk and response (i.e., households, neighborhoods, municipalities, regions) and across the full set of flood-risk drivers that are relevant. For flood-infrastructure investments and flood-risk-reduction measures, sound decision-making also requires knowledge of the effectiveness of different response options, attentive to changes in flood-risk determinants through time—for example, including the ways flood hazards shift under development, impaired maintenance of flood infrastructure, and climate change. To date, however, decision-making across household-to-federal levels has relied on flood hazard maps that do not adequately reflect all flood hazard drivers, nor the ways in which development, stormwater management, and climate change shift patterns of risk through time. Poorly mapped hazards may misinform urban flood risk strategies and lead to maladaptation (Hino & Burke, 2021; Mach et al., 2022; Magnan et al., 2023). This issue is becoming increasingly pressing as flood risks intensify across the U.S. and beyond. Flood maps, such as through FSF, have seemed to fill the flood-map gap, yet with insufficient accuracy in urban areas especially and also with inadequate responsiveness to different scenarios of flood response and development patterns through time. As flood models proliferate, systematic, repeatable methods for comparing the accuracy of flood simulations across them are increasingly essential to develop. It has been suggested that the regional modeling approach used by PRIMo, including the synthesis of local data and the dual-grid model structure, could be applied across every region of the U.S. to more fully understand and respond to flood risks (Bates, 2023b). This becomes possible as several types of data are acquired and organized including accurate, high-resolution topographic data; data describing urban drainage infrastructure such as levees, flood channels, culverts and storm drains; flood channel geometry data (i.e., bathymetric data) and hydrologic data to

analyze extreme events and calibrate models. Our research in Los Angeles also reinforces the importance and potential of collaborative flood modeling to support the build-out, validation and application of these models to meet needs (Mach et al., 2022; Sanders et al., 2023; Ulibarri et al., 2023). Regional-scale collaborative flood modeling could be applied in both urban and rural areas, creating an economy of scale that lowers the overhead necessary for lower-wealth, small communities to have access to fine-resolution flood data for assessing risks and empowers participation in regional planning and adaptation processes. Public access to accurate fine-resolution hazard data, combined with greater public trust in its accuracy, could also help to increase participation in the National Flood Insurance Program, could aid private insurance companies in the identification of insurable properties, and could help property owners to design vulnerability reduction measures such as flood proofing.

It is now well understood that federally defined regulatory floodplains underestimate flood hazards in floodplain communities across the nation (Kelly, 2017). This underestimation results from incomplete inclusion of flood drivers (e.g., precipitation, high tide inundation, climate change) as well as shifts in impervious surface that mean maps may be out of date and, in some cases, sociopolitical negotiation of the flood maps themselves. FSF flood hazard data could be interpreted—and in some cases are being interpreted—as a solution to this underestimation: fine-scale, multi-driver flood hazard data nationwide. However, we demonstrate the risks in adopting FSF hazard data for land-use planning, flood hazard mitigation, insurance and risk transfer, and other flood policies at present —the false precision of the data mean that flood hazards, most especially in urban areas, are not well represented at the scales purported (parcel, block, neighborhood). Practical implementation of our findings takes several forms. First, prioritization of a national framework for regional collaborative flood modeling—as described above —is crucial for actionable flood hazard data products nationwide. Government support for such flood mapping would eliminate problematic issues of limited data access and/or inadequate methodological transparency that can be inherent to private-sector products. Second, selection processes used in state and federal funding programs for flood projects should be cautious about over-reliance on metrics based on FSF data, and consider complementary metrics such as flood losses, physical vulnerabilities in flood infrastructure (e.g., deficient levees), and disadvantaged populations. Third, flood adaptation must be robust to the deeper uncertainties still inherent to flood mapping, under continuing patterns of development and climate change. This can be approached in several ways that don't necessarily require flood maps, such as more stringent rebuild standards after extreme events, limiting severe repetitive loss properties, and conserving and restoring natural infrastructure that buffers communities against flooding.

Data Availability Statement

Data used for this study is available at the following links and repositories:

- The parcel-scale data set containing social data (e.g., population estimates, population fractions by race and ethnicity, and Neighborhood Disadvantage Index (NDI) values) and flood hazard data generated by PRIMo and PRIMo-Drain is accessible at Schubert et al. (2024).
- First Street Foundation flood hazard depth data cannot be made available by the authors based on the terms of the contract for which data were acquired and used. First Street data is available for purchase at https://firststreet.org/data-access.
- Shape files for geolocating the land parcels of Los Angeles County used in this study are available from the Los Angeles County Open Data Portal at this https://data.lacounty.gov/documents/4d67b154ae614d219c58535659128e71/about.
- Census Block Group geometries and select demographic data used to estimate social data by land parcel is available at the following link: https://www.census.gov/geographies/mapping-files/time-series/geo/tiger-data.html.
- American Community Survey Detailed Table Data used to estimate social data by land parcel is available from the U.S. Census Bureau at this link: https://www.census.gov/data/developers/data-sets/acs-5year.2021.html#list-tab-1806015614.
- Locations of storm drains used in PRIMo-Drain is available through the Los Angeles County Storm Drain System at this link: https://pw.lacounty.gov/fcd/stormdrain/disclaimer.cfm?CFID=16930751&CFTOKEN=75ef602ecca4efdd-84A63D53-BAE9-A10E-D4AFC3CC1051325E.
- Matlab scripts for computing exposed populations, exposed property, and Gini indices which quantify social inequalities are presently accessible at Schubert et al. (2024).

Acknowledgments
We express our thanks to the First Street Foundation for making flood hazard data available for this study. We also acknowledge high performance computing support from the NCAR-Wyoming Supercomputing Center provided by the National Science Foundation and the State of Wyoming, and supported by NCAR's Computational and Information Systems Laboratory. We acknowledge comments and suggestions by S.J. Davis and E.-M. Martin which improved the paper, as well as the comments of the reviewers. This work was supported by grants from the National Science Foundation (HDBE-2031535, HDBE-2034308 and SCC-2305476) and the NOAA Effects of Sea Level Rise Program (Grant NA23NOS4780283). B. Sanders and J. Schubert have an equity interest in Zeppelin Floods LLC. This relationship has been reviewed and approved by the University of California, Irvine in accordance with its conflict of interest policies.

References

Alipour, A., Jafarzadegan, K., & Moradkhani, H. (2022). Global sensitivity analysis in hydrodynamic modeling and flood inundation mapping. *Environmental Modelling and Software*, *152*, 105398. https://doi.org/10.1016/j.envsoft.2022.105398

Bates, P. D. (2023a). Fundamental limits to flood inundation modelling. *Nature Water*, *1*(7), 566–567. https://doi.org/10.1038/s44221-023-00106-4

Bates, P. D. (2023b). Uneven burden of urban flooding. *Nature Sustainability*, *6*(1), 9–10. https://doi.org/10.1038/s41893-022-01000-9

Bates, P. D. (2012). Integrating remote sensing data with flood inundation models: How far have we got? *Hydrological Processes*, *26*(16), 2515–2521. https://doi.org/10.1002/hyp.9374

Bates, P. D., Horritt, M. S., & Fewtrell, T. J. (2010). A simple inertial formulation of the shallow water equations for efficient two-dimensional flood inundation modelling. *Journal of Hydrology*, *387*(1–2), 33–45. https://doi.org/10.1016/j.jhydrol.2010.03.027

Bates, P. D., Quinn, N., Sampson, C., Smith, A., Wing, O., Sosa, J., et al. (2021). Combined modeling of U.S. fluvial, pluvial, and coastal flood hazard under current and future climates. *Water Resources Research*, *57*(2). https://doi.org/10.1029/2020WR028673

Bullard, R. D., & Wright, B. (2012). *The wrong complexion for protection: How the government response to disaster endangers African American communities*. New York University Press.

Chakraborty, J., Collins, T. W., & Grineski, S. E. (2019). Exploring the environmental justice implications of hurricane harvey flooding in Greater Houston, Texas. *American Journal of Public Health*, *109*(2), 244–250. https://doi.org/10.2105/AJPH.2018.304846

Conkle, C., Moyer, J., Willardson, B., Walden, A., & Nasseri, I. (2006). *Hydrology manual*. Los Angeles County Department of Public Works. Retrieved from https://dpw.lacounty.gov/wrd/publication/engineering/2006_Hydrology_Manual/2006%20Hydrology%20Manual-Divided.pdf

Council on Environmental Quality. (n.d.). Climate and economic justice screening tool. *Executive Office of the President of the United States. Washington, D.C.* Retrieved from https://screeningtool.geoplatform.gov/en/#7.64/19.637/-115.348

De Moel, H., Jongman, B., Kreibich, H., Merz, B., Penning-Rowsell, E., & Ward, P. J. (2015). Flood risk assessments at different spatial scales. *Mitigation and Adaptation Strategies for Global Change*, *20*(6), 865–890. https://doi.org/10.1007/s11027-015-9654-z

Dottori, F., Di Baldassarre, G., & Todini, E. (2013). Detailed data is welcome, but with a pinch of salt: Accuracy, precision, and uncertainty in flood inundation modeling: OPINION. *Water Resources Research*, *49*(9), 6079–6085. https://doi.org/10.1002/wrcr.20406

Dottori, F., Salamon, P., Bianchi, A., Alfieri, L., Hirpa, F. A., & Feyen, L. (2016). Development and evaluation of a framework for global flood hazard mapping. *Advances in Water Resources*, *94*, 87–102. https://doi.org/10.1016/j.advwatres.2016.05.002

Duncan, B. I., II., Fosmire, E., Butler, A., Warren, H., White, A., Craig, B., et al. (2023). South Carolina strategic statewide resilience and risk reduction plan. *South Carolina Office of Resilience*. Retrieved from https://scor.sc.gov/resilience

Elvidge, C., Tuttle, B., Sutton, P., Baugh, K., Howard, A., Milesi, C., et al. (2007). Global distribution and density of constructed impervious surfaces. *Sensors*, *7*(9), 1962–1979. https://doi.org/10.3390/s7091962

EPA. (2023). EJScreen: Environmental justice screening and mapping tool. Retrieved from https://www.epa.gov/ejscreen

FEMA. (2018). Guidance for flood risk analysis and mapping. In *Flood depth and analysis grids*. Federal Emergency Management Agency. Retrieved from https://www.fema.gov/sites/default/files/2020-02/Flood_Depth_and_Analysis_Grids_Guidance_Feb_2018.pdf

FEMA. (2022). National flood insurance program risk rating 2.0 methodology and data sources. Retrieved from https://www.fema.gov/sites/default/files/documents/FEMA_Risk-Rating-2.0_Methodology-and-Data-Appendix__01-22.pdf

First Street Foundation. (2020). First street foundation flood model, technical methodology document. https://firststreet.org/research-library/flood-model-methodology

Gallegos, H. A., Schubert, J. E., & Sanders, B. F. (2009). Two-dimensional, high-resolution modeling of urban dam-break flooding: A case study of Baldwin Hills, California. *Advances in Water Resources*, *32*(8), 1323–1335. https://doi.org/10.1016/j.advwatres.2009.05.008

Gold, A., Anarde, K., Grimley, L., Neve, R., Srebnik, E. R., Thelen, T., et al. (2023). Data from the drain: A sensor framework that captures multiple drivers of chronic coastal floods. *Water Resources Research*, *59*(4), e2022WR032392. https://doi.org/10.1029/2022WR032392

Harris, L. (2023). Rise of the climate rating agencies. In *The American Prospect*. Retrieved from https://prospect.org/economy/2023-04-12-rise-climate-rating-agencies/

Hino, M., & Burke, M. (2021). The effect of information about climate risk on property values. *Proceedings of the National Academy of Sciences of the United States of America*, *118*(17), e2003374118. https://doi.org/10.1073/pnas.2003374118

Hornbeck, R., & Naidu, S. (2014). When the levee breaks: Black migration and economic development in the American South. *The American Economic Review*, *104*(3), 963–990. https://doi.org/10.1257/aer.104.3.963

Huang, X., & Swain, D. L. (2022). Climate change is increasing the risk of a California megaflood. *Science Advances*, *8*(32), eabq0995. https://doi.org/10.1126/sciadv.abq0995

Jones, L. M. (2018). The big ones: How natural disasters have shaped us (and what we can do about them).

Jonkman, S. N. (2013). Advanced flood risk analysis required. *Nature Climate Change*, *3*(12), 1004. https://doi.org/10.1038/nclimate2031

Kahl, D. T., Schubert, J. E., Jong-Levinger, A., & Sanders, B. F. (2022). Grid edge classification method to enhance levee resolution in dual-grid flood inundation models. *Advances in Water Resources*, *168*, 104287. https://doi.org/10.1016/j.advwatres.2022.104287

Kelly, J. V. (2017). *Fema needs to improve management of its flood mapping programs*. Office of Inspector General, Department of Homeland Security. Retrieved from https://s3.documentcloud.org/documents/4066233/OIG-17-110-Sep17.pdf

Kim, J., Amodeo, M., & Kearns, E. J. (2023). Atlas of probabilistic extreme precipitation based on the early 21st century records in the United States. *Journal of Hydrology: Regional Studies*, *48*, 101480. https://doi.org/10.1016/j.ejrh.2023.101480

Leandro, J., Chen, A. S., Djordjević, S., & Savić, D. A. (2009). Comparison of 1D/1D and 1D/2D coupled (sewer/surface) hydraulic models for urban flood simulation. *Journal of Hydraulic Engineering*, *135*(6), 495–504. https://doi.org/10.1061/(ASCE)HY.1943-7900.0000037

Lindersson, S., Brandimarte, L., Mård, J., & Di Baldassarre, G. (2021). Global riverine flood risk—How do hydrogeomorphic floodplain maps compare to flood hazard maps? *Natural Hazards and Earth System Sciences*, *21*(10), 2921–2948. https://doi.org/10.5194/nhess-21-2921-2021

Los Angeles County. (n.d.). County of Los Angeles open data. *Data Portal for Los Angeles County Data*. County of Los Angeles. Retrieved from https://data.lacounty.gov/

Los Angeles County Public Works. (n.d.). Los Angeles county storm drain system. *Data Portal for Los Angeles County Storm Drain Data*. Retrieved from https://pw.lacounty.gov/fcd/StormDrain/index.cfm

Mach, K. J., Hino, M., Siders, A. R., Koller, S. F., Kraan, C. M., Niemann, J., & Sanders, B. F. (2022). From flood control to flood adaptation. In K. J. Mach, M. Hino, A. R. Siders, S. F. Koller, C. M. Kraan, J. Niemann, et al. (Eds.), *Oxford research encyclopedia of environmental science*. Oxford University Press. https://doi.org/10.1093/acrefore/9780199389414.013.819

Magnan, A. K., Bell, R., Duvat, V. K. E., Ford, J. D., Garschagen, M., Haasnoot, M., et al. (2023). Status of global coastal adaptation. *Nature Climate Change*, *13*(11), 1213–1221. https://doi.org/10.1038/s41558-023-01834-x

Mandli, K. T., & Dawson, C. N. (2014). Adaptive mesh refinement for storm surge. *Ocean Modelling*, *75*, 36–50. https://doi.org/10.1016/j.ocemod.2014.01.002

Molinari, D., De Bruijn, K. M., Castillo-Rodríguez, J. T., Aronica, G. T., & Bouwer, L. M. (2019). Validation of flood risk models: Current practice and possible improvements. *International Journal of Disaster Risk Reduction*, *33*, 441–448. https://doi.org/10.1016/j.ijdrr.2018.10.022
National Research Council (U.S.). (2009). In *Mapping the zone: Improving flood map accuracy*. National Academies Press.
Neal, J., Schumann, G., & Bates, P. (2012). A subgrid channel model for simulating river hydraulics and floodplain inundation over large and data sparse areas. *Water Resources Research*, *48*(11), 2012WR012514. https://doi.org/10.1029/2012WR012514
Nguyen, A.-M., Kim, Y., & Abramson, D. M. (2023). Neighborhood socioeconomic status and women's mental health: A longitudinal study of Hurricane Katrina Survivors, 2005–2015. *International Journal of Environmental Research and Public Health*, *20*(2), 925. https://doi.org/10.3390/ijerph20020925
OCM Partners. (2022). 2015—2016 LARIAC Lidar: Los Angeles Region, CA. Retrieved from https://www.fisheries.noaa.gov/inport/item/55233
O'Donnell, E. C., & Thorne, C. R. (2020). Drivers of future urban flood risk. *Philosophical Transactions of the Royal Society A: Mathematical, Physical & Engineering Sciences*, *378*(2168), 20190216. https://doi.org/10.1098/rsta.2019.0216
Orsi, J. (2004). *Hazardous metropolis: Flooding and urban ecology in Los Angeles*. University of California Press.
Perica, S., Dietz, S., Heim, S., Hiner, L., Maitaria, K., Martin, D., et al. (2014). *NOAA Atlas 14 volume 6 version 2.3, precipitation-frequency Atlas of the United States, California*. NOAA, National Weather Service.
Realtors Property Resource. (n.d.). What is Risk Factor? Retrieved from https://blog.narrpr.com/support/what-is-risk-factor/
Redfin. (2024). Flood Risk Information. Retrieved from https://www.redfin.com/guides/climate-change-housing-impact/flood-risk
Rudari, R., Silvestro, F., Campo, L., Rebora, N., Boni, G., & Herold, C. (2015). *Improvement of the global food model for the GAR 2015 (UNISDR)* [Background Paper prepared for the 2015 Global Assessment Report on Disaster Risk Reduction] (p. 69). CIMA Foundation—Centro Internazionale in Monitoraggio Ambientale Foundation.
Sampson, C. C., Bates, P. D., Neal, J. C., & Horritt, M. S. (2013). An automated routing methodology to enable direct rainfall in high resolution shallow water models. *Hydrological Processes*, *27*(3), 467–476. https://doi.org/10.1002/hyp.9515
Sampson, C. C., Smith, A. M., Bates, P. D., Neal, J. C., Alfieri, L., & Freer, J. E. (2015). A high-resolution global flood hazard model: A high-resolution global flood hazard model. *Water Resources Research*, *51*(9), 7358–7381. https://doi.org/10.1002/2015WR016954
Sanders, B. F., Brady, D., Schubert, J. E., Martin, E.-M. H., Davis, S. J., & Mach, K. J. (2024). Quantifying social inequalities in flood RIsk. *ASCE OPEN: Multidisciplinary Journal of Civil Engineering*, *2*(1). https://doi.org/10.1061/AOMJAH/AOENG-0017
Sanders, B. F., & Grant, S. B. (2020). Re-envisioning stormwater infrastructure for ultrahazardous flooding. *WIREs Water*, *7*(2). https://doi.org/10.1002/wat2.1414
Sanders, B. F., & Schubert, J. E. (2019). PRIMo: Parallel raster inundation model. *Advances in Water Resources*, *126*, 79–95. https://doi.org/10.1016/j.advwatres.2019.02.007
Sanders, B. F., Schubert, J. E., Kahl, D. T., Mach, K. J., Brady, D., AghaKouchak, A., et al. (2023). Large and inequitable flood risks in Los Angeles, California. *Nature Sustainability*, *6*(1), 47–57. https://doi.org/10.1038/s41893-022-00977-7
Savage, J. T. S., Bates, P., Freer, J., Neal, J., & Aronica, G. (2016). When does spatial resolution become spurious in probabilistic flood inundation predictions? *Hydrological Processes*, *30*(13), 2014–2032. https://doi.org/10.1002/hyp.10749
Schubert, J., Sanders, B., & Mach, K. (2024). Comparing first street foundation and PRIMo flood hazard data across the Los Angeles metropolitan region [Dataset]. *DRYAD*. https://doi.org/10.5061/dryad.kd51c5bcz
Serra-Llobet, A., Tourment, R., Montané, A., & Buffin-Belanger, T. (2022). Managing residual flood risk behind levees: Comparing USA, France, and Quebec (Canada). *Journal of Flood Risk Management*, *15*(2), e12785. https://doi.org/10.1111/jfr3.12785
Shu, E. G., Porter, J. R., Hauer, M. E., Sandoval Olascoaga, S., Gourevitch, J., Wilson, B., et al. (2023). Integrating climate change induced flood risk into future population projections. *Nature Communications*, *14*(1), 7870. https://doi.org/10.1038/s41467-023-43493-8
Smiley, K. T. (2020). Social inequalities in flooding inside and outside of floodplains during Hurricane Harvey. *Environmental Research Letters*, *15*(9), 0940b3. https://doi.org/10.1088/1748-9326/aba0fe
Smith, A., Sampson, C., & Bates, P. (2015). Regional flood frequency analysis at the global scale. *Water Resources Research*, *51*(1), 539–553. https://doi.org/10.1002/2014WR015814
Son, Y., Di Lorenzo, E., Park, K., Wipperfurth, S., & Luo, J. (2023). Data assimilation of hyper-local water level sensors for real-time monitoring of coastal inundation. *Coastal Engineering*, *186*, 104398. https://doi.org/10.1016/j.coastaleng.2023.104398
Tate, E., Rahman, M. A., Emrich, C. T., & Sampson, C. C. (2021). Flood exposure and social vulnerability in the United States. *Natural Hazards*, *106*(1), 435–457. https://doi.org/10.1007/s11069-020-04470-2
Trigg, M. A., Birch, C. E., Neal, J. C., Bates, P. D., Smith, A., Sampson, C. C., et al. (2016). The credibility challenge for global fluvial flood risk analysis. *Environmental Research Letters*, *11*(9), 094014. https://doi.org/10.1088/1748-9326/11/9/094014
Ulibarri, N., Valencia-Uribe, C., Sanders, B. F., Schubert, J., Matthew, R., Forman, F., et al. (2023). Framing the problem of flood risk and flood management in metropolitan Los Angeles. *Weather, Climate, and Society*, *15*(1), 45–58. https://doi.org/10.1175/WCAS-D-22-0013.1
U. S. Census Bureau. (2022). Glossary. Retrieved from https://www.census.gov/programs-surveys/geography/about/glossary.html
Vahedifard, F., Azhar, M., & Brown, D. C. (2023). Overrepresentation of historically underserved and socially vulnerable communities behind levees in the United States. *Earth's Future*, *11*(9), e2023EF003619. https://doi.org/10.1029/2023EF003619
Ward, P. J., Jongman, B., Salamon, P., Simpson, A., Bates, P., De Groeve, T., et al. (2015). Usefulness and limitations of global flood risk models. *Nature Climate Change*, *5*(8), 712–715. https://doi.org/10.1038/nclimate2742
Wing, O. E. J., Bates, P. D., Sampson, C. C., Smith, A. M., Johnson, K. A., & Erickson, T. A. (2017). Validation of a 30 m resolution flood hazard model of the conterminous United States. *Water Resources Research*, *53*(9), 7968–7986. https://doi.org/10.1002/2017wr020917
Wing, O. E. J., Lehman, W., Bates, P. D., Sampson, C. C., Quinn, N., Smith, A. M., et al. (2022). Inequitable patterns of US flood risk in the Anthropocene. *Nature Climate Change*, *12*(2), 156–162. https://doi.org/10.1038/s41558-021-01265-6
Wobus, C., Porter, J., Lorie, M., Martinich, J., & Bash, R. (2021). Climate change, riverine flood risk and adaptation for the conterminous United States. *Environmental Research Letters*, *16*(9), 094034. https://doi.org/10.1088/1748-9326/ac1bd7

Erratum

The originally published version of this article contained typographical errors in the Plain Language Summary. In the third sentence, "comparision" should be changed to "comparison." In the fourth sentence, "overliance" should be changed to "overreliance." The errors have been corrected and, this may be considered the authoritative version of record.